# NSIDC Special Report 5
# An Intercomparison of DMSP F11- and F13-derived Sea Ice Products

**Julienne Stroeve, Xiaoming Li, Jim Maslanik**
**May 1997**

**National Snow and Ice Data Center**
**Cooperative Institute for Research in Environmental Sciences**
**University of Colorado, Boulder, Colorado, USA**

## Abstract

Passive microwave satellite data provide an extended time series for monitoring of polar processes, such as variability in sea ice extent. To ensure consistent data sets for time series analysis of sea ice cover, differences between ice concentration estimates from similar sensors on successive spacecraft must be understood. In this study, the effects of changing from the SSM/I F11 to the F13 satellite are examined for a 5-month overlap period. Generally, in terms of hemispheric averages of mean ice concentration, the biases introduced by the switch from F11 to F13 are slight and are not statistically significant; however, in some regions relatively large and significant differences are seen. In addition, differences in sea ice extent and total ice-covered area between the two platforms were found to be statistically significant.

Previous efforts to reduce such differences in geophysical parameters between earlier SSM/Is have focused on establishing relationships between the brightness temperatures. However, we find the relations between the F11 and F13 brightness temperatures to be highly sensitive to the region chosen for the analysis. Consequently, the choice of sample has a substantial effect on the sensor-to-sensor adjustment and on the resulting sea ice concentrations. Furthermore, analysis of ice concentrations between F8 and F11 and between F11 and F13 show that current attempts at a relative calibration of the two instruments do not offer a significant improvement in corresponding ice fractions.

## Introduction

Passive microwave data provide an extended time series for long term monitoring of polar processes, such as variations in sea ice extent. Since 1988, a series of passive microwave sensors - the Defense Meteorological Satellite Programs Special Sensor Microwave/Imager (DMSP SSM/I) - have been used to estimate sea ice cover. While the SSM/Is are of essentially the same design, differences due to sensor calibration and orbit parameters will affect the uniformity of the data set. For time series analyses in particular (e.g. Parkinson and Cavalieri 1989; Parkinson 1992; Johannessen et al. 1995; Maslanik et al. 1996), it is important to understand or at least document relationships between brightness temperatures and ice concentrations (fractional

cover of sea ice) provided by different passive microwave instruments. One means to assess the consistency of the data is through comparisons of brightness temperatures over large homogeneous areas, such as ice sheets (Abdalati et al. 1995; Jezek et al. 1991). Another option is to compare individual orbit antenna temperatures over the open ocean (Wentz, 1995).

In this study, the impact on estimated sea ice concentrations after changing from the DMSP F11 SSM/I to the subsequent F13 SSM/I is assessed for the Arctic and Antarctic. We then attempt to improve the consistency in ice concentrations estimated from F11 and F13 using statistical regression relationships between brightness temperatures for different regions. Next, the impact of the Abdalati et al. (1995) and Wentz (1995) adjustments on the consistency between F8 and F11 sea ice products is reviewed. We conclude by considering the effects of sensor differences on uses of the complete SSM/I time series for polar research.

# Comparison Methods

The DMSP F11 spacecraft was launched into a near polar sun-synchronous orbit on 28 November 1991, with a nominal altitude of 840 km and orbital period of 102 minutes. The DMSP F13 spacecraft was launched on 24 March 1995, also in a near polar sun-synchronous orbit at a nominal altitude of 850 km and orbital period of 102 minutes. The equator crossing time for the ascending node is approximately 6:25 p.m. for F11 and 5:43 p.m. for the F13 satellite. Table 1 summarizes the orbital parameters for the F8, F11 and F13 spacecraft.

The SSM/I instrument as flown on the DMSP spacecraft is a seven channel, four frequency, linearly polarized, passive microwave radiometric system that records emitted energy at 19.3, 22.2, 37.0 and 85.5 GHz. The SSM/I data used here were processed at the National Snow and Ice Data Center in Boulder, Colorado. The final product is a series of daily maps of brightness temperatures for the Northern and Southern hemispheres, gridded into 25 km by 25 km pixels for the 19, 22, and 37 GHz channels, and 12.5 km by 12.5 km pixels at 85 GHz (NSIDC 1996). Since in high latitudes multiple orbit crossings occur over some locations, each pixel consists of an average of all orbit swaths during a 24-hour period.

For the months of May through September 1995, a common data set for the two different SSM/I instruments is available. As indicated in Table 1, the orbit configurations and equator crossing times between F11 and F13 are quite similar, so a reasonable assumption is that any differences between the F11 and F13 brightness temperatures are due primarily to sensor calibration. However, initial examination of the overlapping data showed considerable scatter on specific days. Closer examination of the data for these days indicates that this scatter is due to differences over open ocean areas, resulting from missing orbits in the F11 data. Over such areas, the varying effects of weather over the 24-hour averaging period are substantial enough to introduce considerable differences in the daily averages for F11 and F13. This problem does not affect the systematic sensor-related differences we are considering here, so a visual inspection of brightness temperature scatter plots was used to exclude days with particularly large scatter due to orbit averaging. The end result used for subsequent analysis is a data set of 139 days of overlapping F11 and F13 data, with data excluded for 5 May, 14 July, 1-2 September and 21-22 September.

**Table 1. Comparison of orbital parameters.**

| Parameter | F8 | F11 | F13 |
|---|---|---|---|
| Launch Date | 19 June 1987 | 28 November 1991 | 24 March 1995 |
| Nominal Altitude | 860 km | 840 km | 850 km |
| Inclination Angle | 98.8 degrees | 98.8 degrees | 98.8 degrees |
| Orbital Period | 102 minutes | 102 minutes | 102 minutes |
| Ascending Node Equatorial Crossing (local time) | approximately 6:00 a.m. | approximately 6:25 p.m. | approximately 5:43 p.m. |

To assess the impacts of changing from the F11 to the F13 spacecraft on the derivation of ice fractions, DMSP-F11 and F13 SSM/I daily averaged sea ice concentration grids for the Northern and Southern hemispheres were generated using the NASA Team algorithm (Gloersen and Cavalieri 1986; NSIDC 1996). The existing F11 ice concentration data set archived by NSIDC is based on brightness temperatures adjusted using F8 versus F11 coefficients of Abdalati et al. (1995) applied to the 19, 22 and 37 GHz channels used by the sea ice algorithm. We first adjusted our F11 brightness temperatures in an identical manner. The impact of these adjustments on the F11-F13 comparisons and on F8-F11 differences is discussed in later sections. A weather filter, which uses the 22V and 37V channels, is applied to the data to eliminate most of the spurious ice concentrations resulting from wind-roughening of the ocean surface, cloud liquid water and rainfall (Cavalieri et al. 1995). Cavalieri (1992) discusses the general performance of, and sources of error in, the NASA Team algorithm.

In the following two sections, comparisons are made between total and multiyear ice fractions for the Northern Hemisphere, and between total ice fractions in the Southern Hemisphere. In addition, differences in total ice area and ice extent are evaluated.

# Comparisons of Sea Ice Fraction

## Northern Hemisphere

Table 2 summarizes the comparison of mean monthly total ice concentrations derived from F11 and F13 in terms of mean difference, standard deviation, root-mean-squared (r.m.s.) error and correlation, respectively.

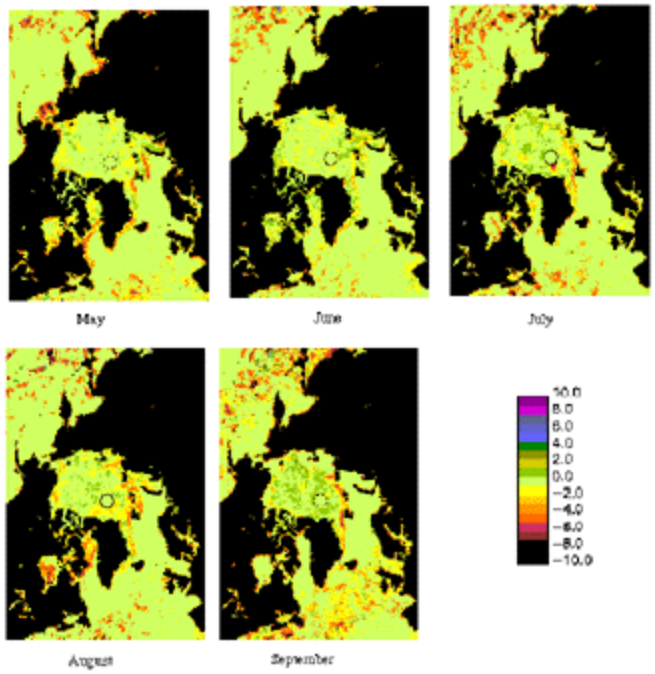


Figure 1. Monthly spatial patterns of Northern Hemisphere total ice concentration differences.

The equations of linear least squares best fit are also given in Table 2. The statistics are computed for the Northern Hemisphere sea ice with and without an expanded land mask. As noted later, the largest differences occur along coastlines as a result of geolocation uncertainty and false retrievals of ice cover in open-ocean coastal pixels due to mixed-pixel effects from adjoining land (land contamination). A land mask expanded to 3 pixels out from the original land mask was used to minimize these effects. Table 2 lists the comparison results using the regular and expanded land mask. An additional calculation was performed for the central Arctic region, where any contaminated land pixels were filtered out using the expanded land mask.

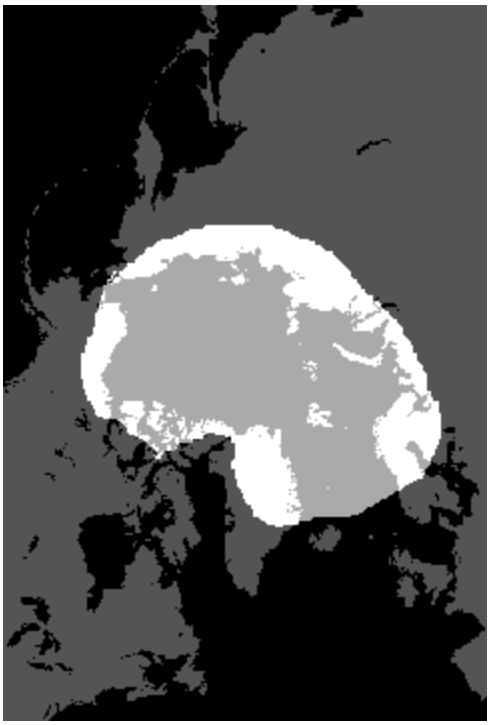

Figure 2. Location of the area defined as the central Arctic.

The effects of changing satellites on the overall monthly mean total sea ice concentrations are, in general, minimal. The differences in monthly mean total sea ice between the two satellites is less than 10 percent in all cases, and within one percent in most cases. There are, however, some larger regional differences in sea ice concentration between the two satellites which are most pronounced in the Barents Sea during May and July, and appear in all months in the North and East Greenland seas. In these regions, F11-derived sea ice fractions are consistently greater than those from F13 by approximately three to six percent (absolute). Large differences can also be found along the ice margins, particularly during the months of May, July and September.

The greatest differences in total ice concentration between the two satellites are found over the open ocean and along coastlines. The magnitude of open ocean differences are randomly distributed and believed to be an artifact of weather effects not fully eliminated by the weather filter. Land contamination and geolocation errors also lead to similar discrepancies. Geolocation accuracy for these data are estimated to be approximately 5 km (F. Wentz, personal communication). Total ice concentration differences in the Barents Sea, north and east Greenland seas, along the coastlines and over the open ocean, as well as a few pixels in the interior and edge of the ice pack, are statistically significant at a 99 percent confidence level.

Table 2 shows that except for the month of May, F13 mean monthly total ice differences as averaged over the entire Northern Hemisphere are slightly higher than those from F11. Using the expanded land mask, F11 data yield slightly higher total ice fractions during May and July. The use of an expanded land mask improves the performance, relative to F11, in total sea ice fractions, as seen by a reduction in the mean difference, standard deviation and r.m.s. error. Thus, as has been noted for differences between Scanning Multichannel Microwave Radiometer (SMMR) and SSM/I F8 data (Maslanik et al. 1996), a large part of the overall mean difference in

total ice fractions between the satellites occurs along the coasts as a result of land contamination accentuated by geolocation differences.

If we restrict the analysis to the central Arctic, a further reduction in mean difference, standard deviation and r.m.s. error is observed relative to Northern Hemisphere ice fractions using the regular land mask and in some cases, using the expanded land mask. In this region, F13 total ice concentrations remain slightly greater than those from F11 for the five months analyzed. The reason for the smaller mean differences is that this region does not contain the relatively large biases observed over the open ocean and along coasts.

In Table 3, we compare F11 and F13 total ice fractions averaged over the entire 139 day time period, and the spatial patterns of the mean differences are shown in Figure 3 [a].

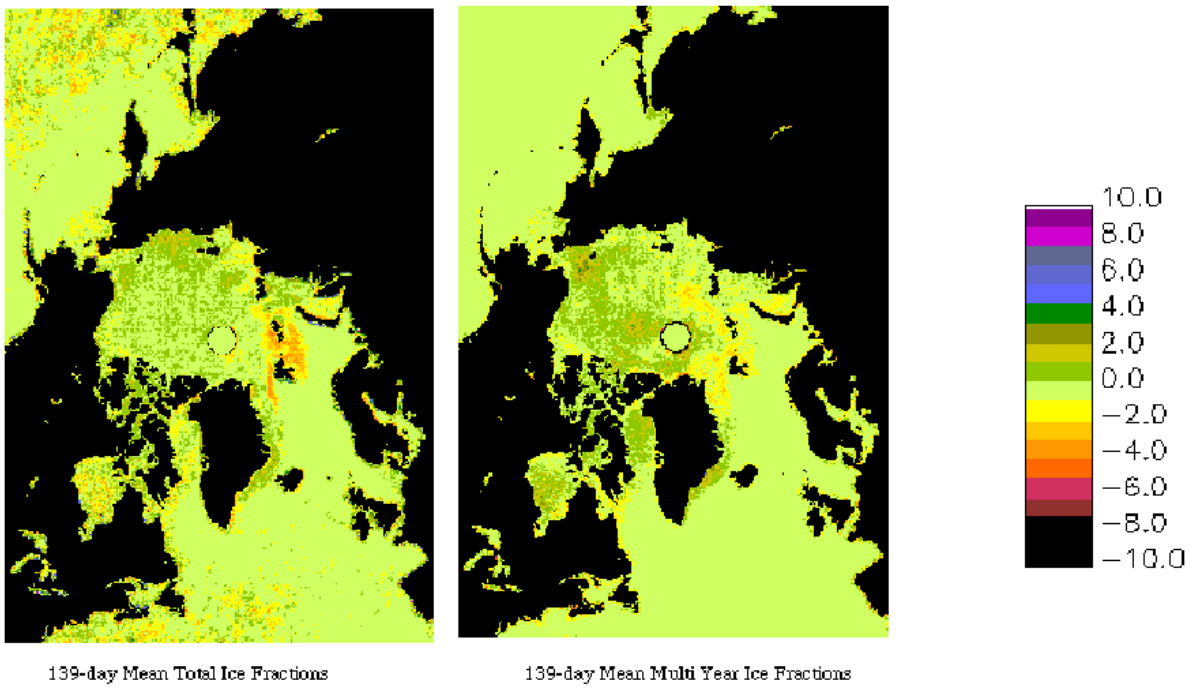


Figure 3 [a] and [b]. Overall mean (139-day) spatial patterns of Northern Hemisphere total and multiyear ice concentration differences.

In general it can be said that somewhat greater total ice fractions can be expected using the F13 satellite data during Northern Hemisphere summer, with respect to those from F11. In the North and East Greenland seas however, F11 total ice concentrations remain consistently greater that those from F13. One possible explanation for these differences may be that geolocation and orbital differences result in systematic brightness temperature differences, and hence ice concentration differences in these regions. An inspection of the brightness temperature difference patterns, particularly at 19H, reveal that the F11 brightness temperatures are consistently greater than those from F13 by as much as 5 K in the Greenland Sea. Overall however, the mean difference between the two satellites remains well below one percent. These differences are reduced by minimizing the effects of land contamination and weather over open ocean.

In the case of multiyear ice (MYI) fractions, similar discrepancies are observed (Figure 4).

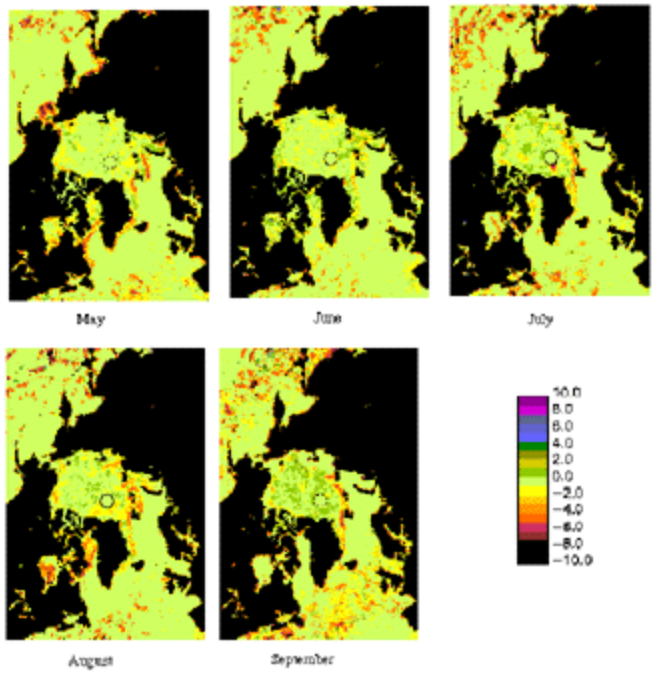


Figure 4. Monthly spatial patterns of Northern Hemisphere multiyear ice concentration differences.

Since differences between F11 and F13 brightness temperatures are greater between frequencies (37 GHz vs. 19 GHz) than between polarizations (19 GHz vertical polarization [19v] and 19 GHz horizontal polarization [19h]), somewhat larger monthly mean differences are observed for multiyear than for total ice. The impact of changing from the F11 to the F13 satellite is an increase in the apparent MYI fraction (positive mean difference) for all months except September (see Table 4). The F11-derived MYI estimates are consistently higher than those from the F13 satellite in the north and east Greenland seas, and along the ice edge. The differences in these locations range between two to six percent, and are statistically significant at a confidence level of 99 percent. However, there are instances where F13 MYI fractions are greater than those from F11 by six to 10 percent.

**Table 2. Comparison of F11 and F13 monthly mean total ice concentrations (F13 minus F11). Coefficients of linear least squares best fit are also given, where x = F11, y = F13.**

| Month | Mean Difference (%) | Standard Deviation (%) | r.m.s. error %) | Correlation Coefficient (r) | Slope | Intercept (K) |
|---|---|---|---|---|---|---|
| **Northern Hemisphere - expanded land mask** | | | | | | |
| May | -0.059 | 1.025 | 1.025 | 0.999 | 1.000 | -0.065 |
| June | -0.095 | 1.020 | 1.014 | 0.999 | 1.003 | 0.038 |
| July | -0.035 | 1.216 | 1.216 | 0.999 | 1.000 | -0.036 |

| | | | | | | |
|---|---|---|---|---|---|---|
| August | 0.002 | 1.293 | 1.289 | 0.999 | 1.004 | -0.037 |
| September | 0.104 | 1.463 | 1.459 | 0.998 | 1.004 | -0.062 |
| **Northern Hemisphere - regular land mask** | | | | | | |
| May | -0.034 | 1.368 | 1.368 | 0.999 | 1.000 | -0.037 |
| June | 0.252 | 1.462 | 1.456 | 0.999 | 1.004 | 0.164 |
| July | 0.114 | 1.778 | 1.778 | 0.998 | 1.000 | 0.112 |
| August | 0.182 | 1.972 | 1.970 | 0.998 | 1.004 | 0.132 |
| September | 0.124 | 1.891 | 1.887 | 0.998 | 1.005 | 0.060 |
| **Central Arctic** | | | | | | |
| May | 0.036 | 0.849 | 0.845 | 0.999 | 1.002 | -0.113 |
| June | 0.217 | 0.762 | 0.758 | 0.999 | 1.002 | 0.099 |
| July | 0.027 | 0.928 | 0.921 | 0.999 | 1.003 | -0.122 |
| August | 0.216 | 0.931 | 0.920 | 0.999 | 1.004 | 0.073 |
| September | 0.210 | 0.981 | 0.944 | 0.999 | 1.007 | -0.042 |

**Table 3. Comparison of F11 and F13 139-day mean total ice concentrations (F13 minus F11). Coefficients of linear least squares best fit are also given, where x = F11, y = F13.**

| Description | Mean Difference (%) | Standard Deviation (%) | r.m.s. error %) | Correlation Coefficient (r) | Slope | Intercept (K) |
|---|---|---|---|---|---|---|
| Northern Hemisphere - expanded mask | 0.042 | 0.667 | 1.654 | 0.999 | 1.005 | -0.022 |
| Northern Hemisphere - regular mask | 0.169 | 1.027 | 1.014 | 0.999 | 1.005 | 0.065 |
| Central Arctic | 0.209 | 0.804 | 0.779 | 0.999 | 1.005 | -0.068 |

These differences occur during the month of May in the Denmark Strait, Baffin Bay and Chukchi Sea, during the month of June in the Chukchi Sea and Hudson Bay, and near the pole during July and August.

Unlike the comparisons of total ice concentration, the MYI differences between the two satellites are minimal over the open ocean (e.g., weather effects result in false estimates of first-year ice rather than multiyear ice). Thus, the mean difference, standard deviation and r.m.s. error all increase when limiting the analysis to the central Arctic. As noticed previously in total ice fractions, the lowest mean differences, standard deviations and r.m.s. errors are observed when large differences along coasts and near the pole are removed using the expanded land mask.

Figure 3 [b] shows spatial patterns of the 139-day mean multiyear ice concentration differences between F13 and F11, and the statistics are given in Table 5.

F11 MYI fractions remain slightly larger than those from F13 by two to three percent, and less than those from F13 by a similar magnitude near the pole. Excluding a few points near the pole where orbital differences cause larger discrepancies along the edges of orbit coverage centered around the pole, the maximum difference between the 139-day mean F11 and F13 multiyear sea ice concentrations is six percent (see Figure 4). Elsewhere, the maximum differences are found near the coasts as a result of land contamination and/or geolocation errors.

It is worth noting that there are individual days with total and multiyear ice differences as large as 30 percent (absolute). One explanation for the larger deviations found on a few days could be missing orbits that bias the daily averages. The impact of missing orbits is expected to be most pronounced in the marginal ice zone where ice conditions change rapidly. It is in these areas of low ice concentration where the largest discrepancies between the two satellites are observed. The magnitude of the differences decreases in the 139-day mean estimate of sea ice fractions.

**Table 4. Comparison of F11 and F13 monthly mean multiyear ice concentrations (F13 minus F11). Coefficients of linear least squares best fit are also given, where x = F11, y = F13.**

| Month | Mean Difference (%) | Standard Deviation (%) | r.m.s. error %) | Correlation Coefficient (r) | Slope | Intercept (K) |
|---|---|---|---|---|---|---|
| **Northern Hemisphere - expanded land mask** | | | | | | |
| May | 0.103 | 0.949 | 0.916 | 0.997 | 1.019 | -0.014 |
| June | 0.281 | 1.049 | 0.991 | 0.989 | 1.054 | 0.136 |
| July | -0.071 | 0.511 | 0.441 | 0.981 | 1.129 | 0.004 |
| August | 0.049 | 0.649 | 0.626 | 0.997 | 1.020 | -0.003 |
| September | -0.063 | 0.052 | 0.516 | 0.999 | 0.994 | -0.033 |
| **Northern Hemisphere - regular land mask** | | | | | | |
| May | 0.092 | 1.257 | 1.245 | 0.996 | 1.014 | -0.008 |
| June | 0.352 | 1.228 | 1.185 | 0.984 | 1.051 | 0.188 |

| | | | | | | |
|---|---|---|---|---|---|---|
| July | 0.085 | 0.779 | 0.776 | 0.967 | 1.050 | 0.033 |
| August | 0.088 | 1.167 | 1.139 | 0.994 | 1.025 | -0.001 |
| September | -0.147 | 0.888 | 0.886 | 0.999 | 0.996 | -0.123 |
| **Central Arctic** | | | | | | |
| May | 0.391 | 1.287 | 1.209 | 0.997 | 1.027 | -0.134 |
| June | 0.701 | 1.286 | 1.256 | 0.991 | 1.030 | 0.393 |
| July | 0.305 | 0.957 | 0.832 | 0.980 | 1.132 | 0.038 |
| August | 0.197 | 1.283 | 1.247 | 0.994 | 1.021 | 0.016 |
| September | -0.233 | 0.970 | 0.970 | 0.999 | 0.997 | -0.170 |

**Table 5. Comparison of F11 and F13 139-day mean multiyear ice concentrations (F13 minus F11). Coefficients of linear least squares best fit are also given, where x = F11, y = F13.**

| Description | Mean Difference (%) | Standard Deviation (%) | r.m.s. error %) | Correlation Coefficient (r) | Slope | Intercept (K) |
|---|---|---|---|---|---|---|
| Northern Hemisphere - expanded mask | 0.095 | 0.465 | 1.434 | 0.999 | 1.021 | 0.026 |
| Northern Hemisphere - regular mask | 0.092 | 0.683 | 0.673 | 0.997 | 1.014 | 0.033 |
| Central Arctic | 0.263 | 0.780 | 0.747 | 0.998 | 1.019 | 0.028 |

## Southern Hemisphere

In the Southern Hemisphere, the largest differences between the F11 and F13 ice fractions are observed during the month of May, with differences along the ice margin as great as six to 10 percent (F13 F11) (Figure 5).

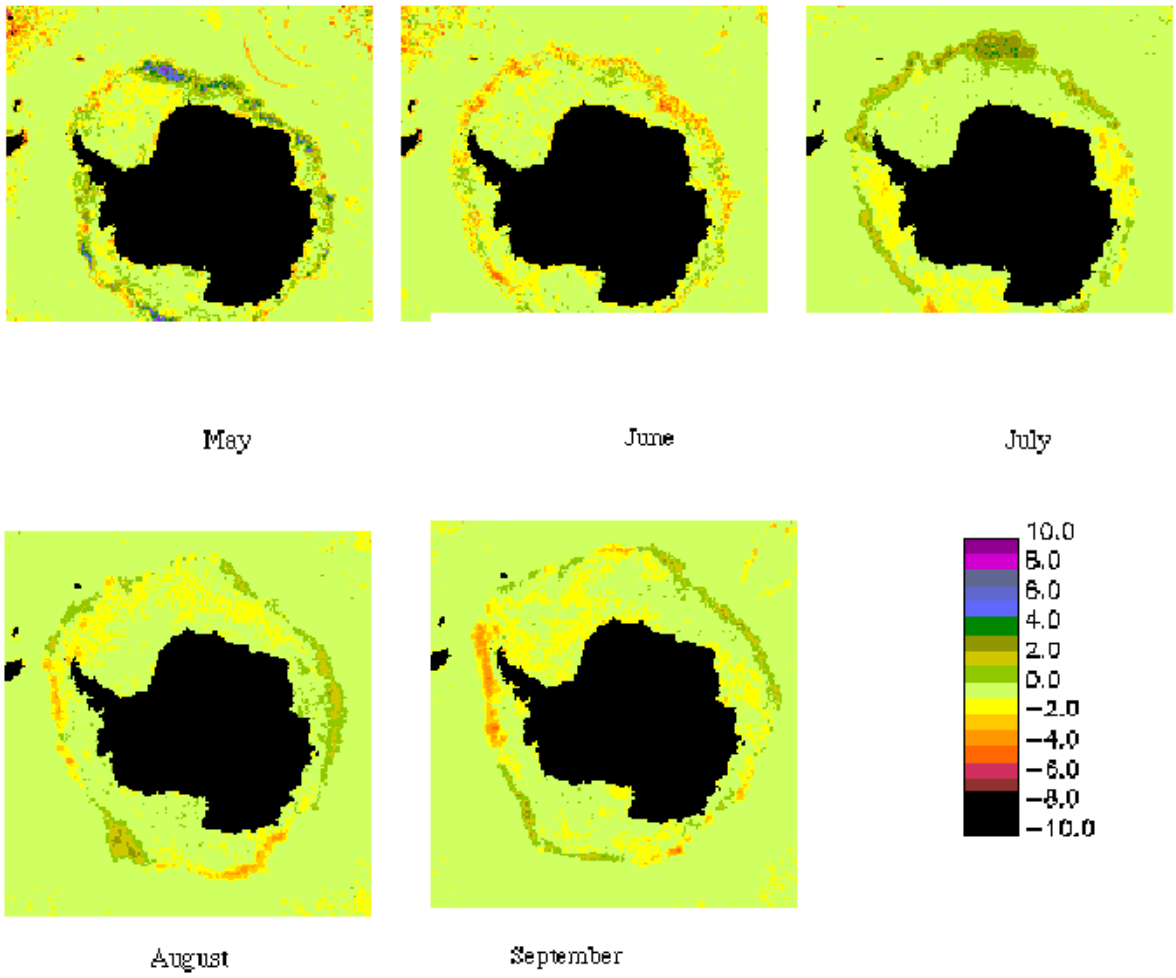


Figure 5. Monthly spatial patterns of Southern Hemisphere total ice concentration differences.

During the other months, the F13 concentrations are in general slightly greater than those from F11 (one to four percent) along the ice margin, whereas at the edge of the Antarctic continent, F11 concentrations are somewhat greater (one to three percent). Differences of a similar magnitude are observed over the open ocean, but they are not as great as in the Northern Hemisphere because weather effects due to atmospheric water content are less during polar winter. Also, since diurnal variability is less during winter, errors resulting from missing orbits should be reduced.

Table 6 summarizes the comparison between F11 and F13 monthly mean ice concentrations for the Southern Hemisphere using a regular and expanded land mask. The overall greatest monthly mean differences, standard deviation and r.m.s. error occur during May, where F13 ice fractions are approximately 0.3 percent greater than those from F11. With the expanded land mask, there are essentially no statistical differences between the F11 and F13 ice concentrations.

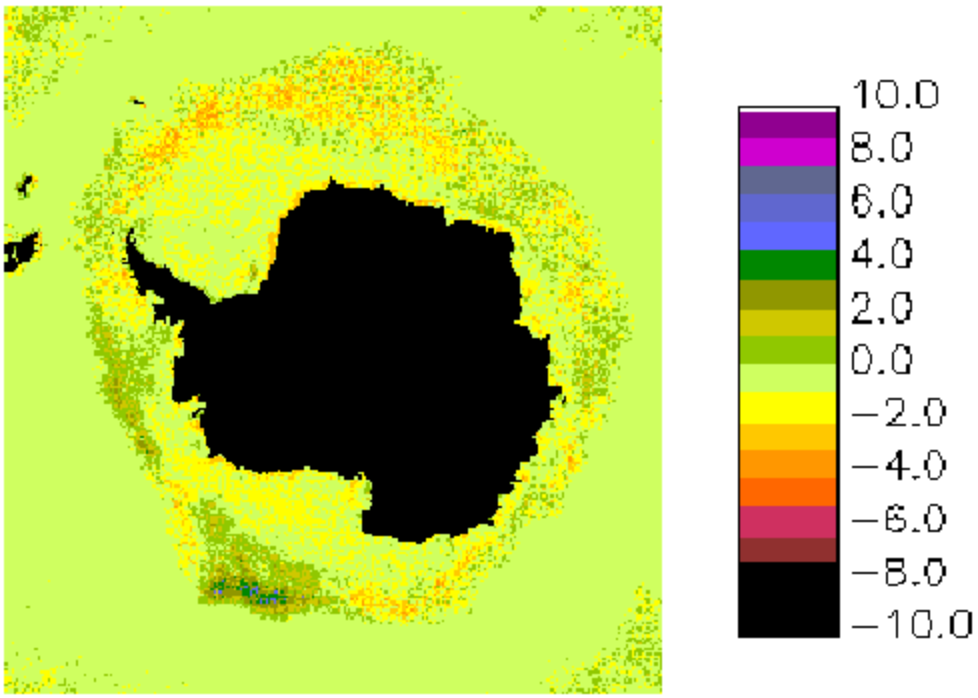


Figure 6. Overall mean (139-day) spatial patterns of Southern Hemisphere total ice concentration differences.

In terms of the overall 139-day mean total ice fractions, the maximum difference in sea ice concentration between the two satellites is six percent and occurs over the open ocean (Figure 6) and the F11 ice fractions for the Southern Hemisphere are on average only 0.01 percent greater than those from F13 for the 139-day mean comparison (Table 7).

**Table 6. Comparison of F11 and F13 mean monthly total ice concentrations (F13 minus F11). Coefficients of linear least squares best fit are also given, where x = F11, y = F13.**

| Month | Mean Difference (%) | Standard Deviation (%) | r.m.s. error %) | Correlation Coefficient (r) | Slope | Intercept (K) |
|---|---|---|---|---|---|---|
| **Southern Hemisphere - expanded land mask** | | | | | | |
| May | 0.273 | 1.141 | 1.111 | 0.999 | 1.008 | 0.142 |
| June | 0.071 | 0.654 | 0.652 | 0.999 | 1.002 | 0.036 |
| July | 0.152 | 0.704 | 0.702 | 0.999 | 1.002 | 0.115 |
| August | 0.065 | 0.536 | 0.535 | 0.999 | 1.004 | -0.037 |
| September | 0.013 | 0.541 | 0.540 | 0.999 | 0.999 | 0.037 |
| **Southern Hemisphere - regular land mask** | | | | | | |

| | | | | | | |
|---|---|---|---|---|---|---|
| May | 0.273 | 1.147 | 1.120 | 0.999 | 1.008 | 0.143 |
| June | 0.071 | 0.664 | 0.661 | 0.999 | 1.002 | 0.036 |
| July | 0.151 | 0.702 | 0.700 | 0.999 | 1.001 | 0.115 |
| August | 0.066 | 0.535 | 0.534 | 0.999 | 1.001 | 0.046 |
| September | 0.011 | 0.540 | 0.539 | 0.999 | 0.999 | 0.037 |

**Table 7. Comparison of F11 and F13 139-day mean total ice concentrations (F13 minus F11). Coefficients of linear least squares best fit are also given, where x = F11, y = F13.**

| Description | Mean Difference (%) | Standard Deviation (%) | r.m.s. error %) | Correlation Coefficient (r) | Slope | Intercept (K) |
|---|---|---|---|---|---|---|
| Southern Hemisphere - expanded mask | 0.014 | 0.671 | 1.663 | 0.999 | 0.997 | 0.068 |
| Southern Hemisphere - regular mask | 0.015 | 0.679 | 0.670 | 0.999 | 0.997 | 0.069 |

# Comparisons of Total Ice-Covered Area and Ice Extent

Investigations of trends in sea ice cover often include summaries of total area covered by sea ice (total ice-covered area) and total area with at least some sea ice coverage (total ice extent). In this section the effect on these measures of changing from SSM/I F11 to F13 is examined. Here, total ice extent is computed by summing the total number of pixels with at least 15 percent ice concentration multiplied by the area per pixel (25 km x 25 km). Total ice-covered area is defined as the area of the pixels with at least 15 percent ice concentration multiplied by the ice concentration in the pixel (0.15 - 1.00). Total sea ice area and ice extent for the Northern Hemisphere, central Arctic and Southern Hemisphere were computed for each day. The monthly means are presented in Tables 8 and 9 for monthly ice extents and covered areas, respectively, and 139-day means are given in Table 10.

In both hemispheres, F13-derived total ice extent is greater than that from F11. This is a result of fewer F13 pixels classified as open water by the weather filter. Except during May, August and September in the Northern Hemisphere averages, the differences in sea ice extent are statistically significant for a 99 percent confidence level. All the monthly sea ice extent differences in the Southern Hemisphere are statistically significant for a 99 percent confidence level. Since the greatest discrepancies between the two satellites are observed over the Northern

Hemisphere open ocean, the agreement in ice extent improves when restricting the analysis region to the central Arctic, although the differences remain significant for all months except May.

The agreement between the two satellites improves when examining differences in total ice-covered area, as seen by a reduction in the percent mean differences. However, the differences do remain statistically significant for a 99 percent confidence level, during May and June in the Northern Hemisphere, during May, June and July in the central Arctic, and for all months in the Southern Hemisphere.

An inspection of the overall (139-day) mean differences in total ice covered area and sea ice extent reveal that there is good agreement in the total ice covered area, but significant differences remain when comparing ice extent. Overall, switching from the F11 to the F13 spacecraft will result in slightly higher estimates of ice covered area and ice extent. These differences however, remain below one percent, which are on the order of trends observed for the central Arctic and Antarctica.

**Table 8. Comparison of mean differences in sea ice extent between the F13 and F11 satellites (F13 minus F11). The paired t-test statistic is also given in the table.**

| Month | Mean Difference ($km^2$) | Standard Deviation ($km^2$) | Minimum Difference ($km^2$) | Maximum Difference ($km^2$) | t-value |
|---|---|---|---|---|---|
| **Northern Hemisphere** | | | | | |
| May | 3,080 ( 0.05%) | 38,442 | -106,250 | 95,000 | 0.42 |
| June | 14,208 ( 0.23%) | 72,359 | - 88,125 | 292,500 | 2.64 |
| July | 45,841 ( 0.91%) | 37,960 | -15,625 | 128,750 | 6.16 |
| August | 16,542 ( 0.42%) | 41,498 | -97,500 | 86,875 | 2.18 |
| September | 23,773 ( 0.60%) | 98,137 | -199,375 | 343,750 | 1.26 |
| **Central Arctic** | | | | | |
| May | - 1,473 (-0.03%) | 4,240 | -12,500 | 8,125 | -1.84 |
| June | 5,687 ( 0.11%) | 7,657 | - 6,250 | 28,750 | 4.07 |
| July | 23,125 ( 0.50%) | 6,803 | 11,250 | 39,375 | 17.34 |
| August | 16,499 ( 0.43%) | 12,353 | - 5,625 | 47,500 | 7.31 |
| September | - 5,069 (-0.14%) | 7,424 | -18,125 | 8,750 | -3.55 |
| **Southern Hemisphere** | | | | | |

| | | | | | |
|---|---|---|---|---|---|
| May | 46,340 ( 0.53%) | 72,359 | - 88,15 | 292,500 | 3.39 |
| June | 79,104 ( 0.64%) | 101,096 | - 75,625 | 523,750 | 4.29 |
| July | 6,436 ( 0.47%) | 84,691 | -125,000 | 284,375 | 3.87 |
| August | 59,166 ( 0.38%) | 61,851 | - 30,625 | 224,375 | 5.24 |
| September | 77,500 ( 0.44%)` | 49,839 | - 25,625 | 167,500 | 8.08 |

**Table 9. Comparison of mean differences in total ice covered area between the F13 and F11 satellites (F13 minus F11). The paired t-test statistic is also given in the table.**

| Month | Mean Difference ($km^2$) | Standard Deviation ($km^2$) | Minimum Difference ($km^2$) | Maximum Difference ($km^2$) | t-value |
|---|---|---|---|---|---|
| **Northern Hemisphere** | | | | | |
| May | 13,004 ( 0.23%) | 14,570 | - 6,520 | 50,780 | 4.72 |
| June | 12,839 ( 0.24%) | 22,089 | - 48,581 | 55,270 | 3.11 |
| July | - 3,513 (-0.09%) | 27,747 | - 58,600 | 51,399 | -0.65 |
| August | -11,648 (-0.40%) | 34,219 | -106,240 | 57,700 | -1.86 |
| September | 12,888 ( 0.44%) | 39,902 | - 59,950 | 96,480 | 1.68 |
| **Central Arctic** | | | | | |
| May | 8,775 (0.19%) | 8,423 | - 2,610 | 34,030 | 5.51 |
| June | 10,731 (0.23%) | 7,796 | -12,750 | 27,040 | 7.54 |
| July | -8,069 (-0.22%) | 11,881 | -25,009 | 17,330 | - 3.46 |
| August | -4,321 (-0.15%) | 12,450 | -41,030 | 15,690 | - 1.91 |
| September | - 770 (-0.03%) | 8,270 | -12,590 | 24,820 | - 0.48 |
| **Southern Hemisphere** | | | | | |
| May | 39,253 ( 0.57%) | 20,289 | 10,450 | 88,470 | 10.24 |
| June | 58,692 ( 0.60%) | 33,023 | - 45,120 | 168,310 | 9.73 |
| July | -24,228 (-0.22%) | 25,967 | -718,000 | 16,000 | - 4.76 |

| | | | | | |
|---|---|---|---|---|---|
| August | -28,567 (-0.23%) | 30,546 | -101,300 | 32,900 | - 5.12 |
| September | -33,321 (-0.24%) | 24,190 | - 86,000 | 4,300 | - 7.16 |

**Table 10. Comparison of 139-day mean differences in total ice covered area and ice extent between the F13 and F11 satellites (F13 minus F11). The paired t-test statistic is also given in the table.**

| Area | Mean Difference ($km^2$) | Standard Deviation ($km^2$) | Minimum Difference ($km^2$) | Maximum Difference ($km^2$) | t-value |
|---|---|---|---|---|---|
| **Ice Area** | | | | | |
| Northern Hemisphere | 4,434 (0.11%) | 30,504 | -96,480 | 106,240 | 1.72 |
| Central Arctic | 1,512 (0.04%) | 12,298 | -41,030 | 34,030 | 1.45 |
| Southern Hemisphere | 3,906 (0.04%) | 47,269 | -101,300 | 168,310 | 0.98 |
| **Ice Extent** | | | | | |
| Northern Hemisphere | 20,223 (0.40%) | 55,517 | -199,375 | 343,750 | 11.31 |
| Central Arctic | 7,906 (0.17%) | 13,118 | - 15,625 | 47,500 | 7.13 |
| Southern Hemisphere | 65,107 (0.48%) | 76,461 | -125,000 | 523,750 | 10.08 |

# Brightness Temperature Comparisons

Abdalati et al. (1995) examined the correlation between F8 and F11-SSM/I brightness temperatures using 24-hour averaged brightness temperatures archived at NSIDC. The regions chosen for the analysis were the Greenland and Antarctic ice sheets, as they exhibit spatial homogeneity and a weak diurnal cycle, and thus should highlight calibration differences between F8 and F11. Small variations between the F8 and F11 data sets were attributed to different orbital characteristics, especially time differences of the two satellites (refer to Table 1). On the basis of this analysis, Abdalati et al. (1995) obtained a set of regression coefficients to adjust the F11 brightness temperatures in the 19, 22 and 37 GHz channels to correspond more closely to those of F8.

The purpose of this adjustment was to maximize the consistency of the F8 and F11 brightness temperature time series for analysis of Greenland ice sheet conditions. However, since application of the regression coefficients also resulted in a reported decrease in the differences between F8 and F11 sea ice concentrations, this adjustment was adopted for the operational production of sea ice products at NSIDC. Here, we consider a similar approach for the F11 and F13 satellites, with the particular goal of improving the consistency in the above mentioned ice concentrations estimated from F11 and F13.

First, comparison regions were selected from both the Northern and Southern hemispheres as shown in Figures 7 [a] and [b].

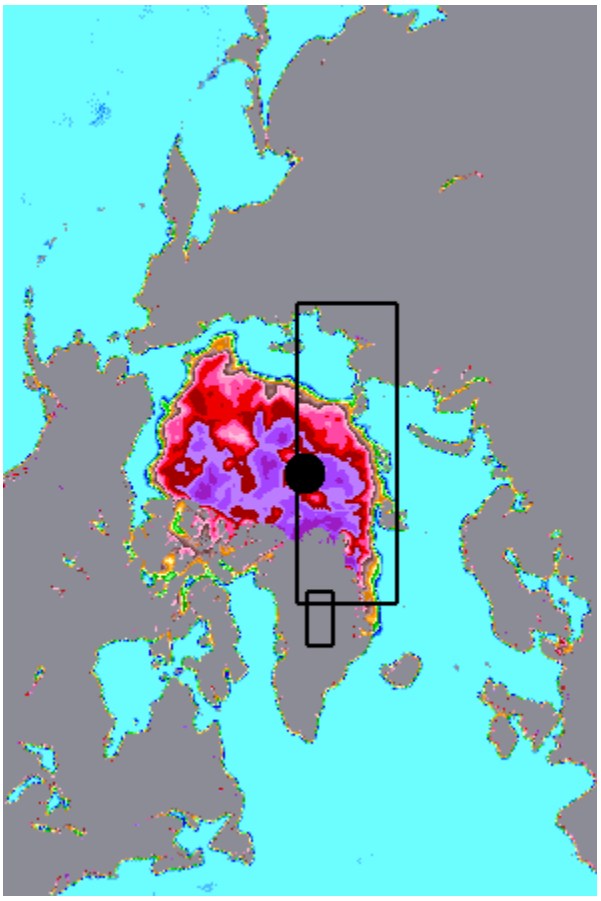

Figure 7[a]. Regions selected in the Northern Hemisphere for the brightness temperature comparison.

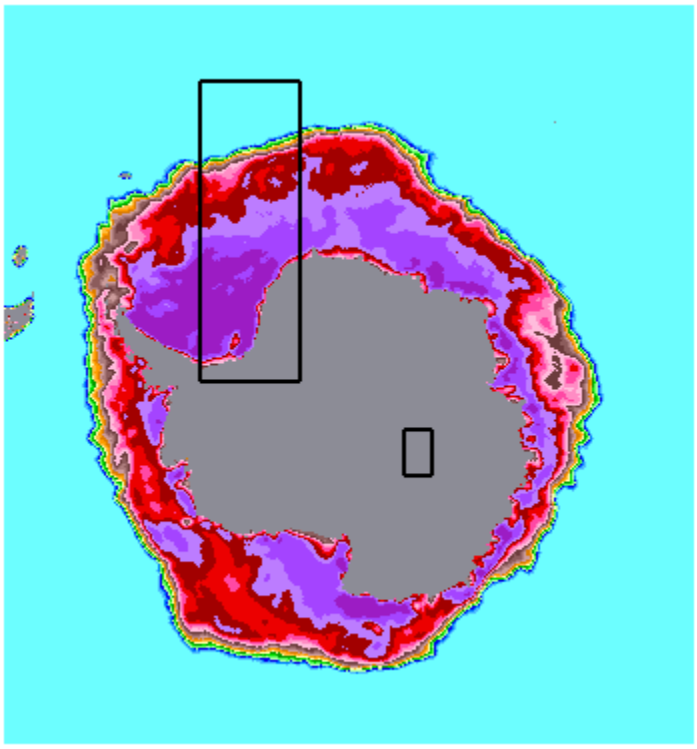

Figure 7[b]. Regions selected in the Southern Hemisphere for the brightness temperature comparison.

These regions include sea-ice areas as well as areas from the Greenland and Antarctic ice sheets. The area over Greenland consists of 351 pixels selected for an area with an altitude above 2000m, resulting in 29,133 measurements over an 83-day overlap period (July through September). Surface elevations higher than 2000m were chosen to avoid melt events near the coast that could result in large diurnal variations in brightness temperatures. Over Antarctica, the area comprises 322 pixels, yielding 26,726 pixels for the overlap period. The F11 and F13 brightness temperatures for the ice sheet regions were analyzed individually and in combination.

An analysis was also made of brightness temperatures over sea ice. For the Northern Hemisphere, this amounted to a total of 561,701 pixels, and 583,238 pixels for the Southern Hemisphere. Finally, with the intent of developing a more globally applicable set of regression coefficients, a comparison of all brightness temperatures for the Northern Hemisphere and Southern Hemisphere, averaged over the 83-day data set, was performed. This comparison includes not only ice sheets and sea ice, but open ocean and land as well. Assuming that variations in brightness temperatures between the two satellites, such as those due to differences in equator crossing times, are randomly distributed, any resulting differences in mean brightness temperatures can be attributed to relative calibration differences. This method is an alternative to analyzing brightness temperatures on an individual orbit basis, which at this point was not feasible.

As with the ice concentration comparisons described earlier, brightness temperatures from F11 and F13 were compared using difference maps, scatter plots and regression. The results of the regression analysis for the different regions are listed in Table 11. The F11 brightness

temperatures are taken as the independent variable and the F13 values as the dependent variable. The F11 instrument was chosen as the baseline instrument in order to maintain consistency with the previous work by Abdalati et al. (1995), with the F11 brightness temperatures adjusted via regression coefficients to correspond to those of F8.

**Table 11. The results of the regression analysis for the different regions based on comparisons from F11 and F13.**

| ***19h*** | **Intercept (K)** | **Slope** | **Correlation Coefficient (r)** |
|---|---|---|---|
| Greenland Ice Sheet | 2.705 | 0.985 | 0.994 |
| Antarctic Ice Sheet | 1.554 | 0.988 | 0.998 |
| Greenland and Antarctic Ice Sheets | -0.604 | 1.003 | 0.999 |
| Northern Hemisphere Sea Ice | 2.179 | 0.986 | 0.997 |
| Southern Hemisphere Sea Ice | 3.554 | 0.982 | 0.997 |
| Mean Northern Hemisphere | 1.633 | 0.995 | 0.997 |
| Mean Southern Hemisphere | -0.59 | 1.003 | 0.999 |
| Mean Northern and Southern Hemispheres | 0.307 | 0.999 | 0.998 |
| ***19v*** | **Intercept (K)** | **Slope** | **Correlation Coefficient (r)** |
| Greenland Ice Sheet | 4.875 | 0.977 | 0.993 |
| Antarctic Ice Sheet | 1.186 | 0.992 | 0.998 |
| Greenland and Antarctic Ice Sheets | 0.606 | 0.996 | 0.999 |

| | | | |
|---|---|---|---|
| Northern Hemisphere Sea Ice | 0.901 | 0.994 | 0.996 |
| Southern Hemisphere Sea Ice | 2.177 | 0.989 | 0.996 |
| Mean Northern Hemisphere | 1.09 | 0.996 | 0.992 |
| Mean Southern Hemisphere | 1.282 | 0.993 | 0.999 |
| Mean Northern and Southern Hemispheres | 2.084 | 0.991 | 0.991 |
| ***22v*** | **Intercept (K)** | **Slope** | **Correlation Coefficient (r)** |
| Greenland Ice Sheet | 7.52 | 0.964 | 0.987 |
| Antarctic Ice Sheet | 2.179 | 0.986 | 0.998 |
| Greenland and Antarctic Ice Sheets | 1.327 | 0.991 | 0.999 |
| Northern Hemisphere Sea Ice | 3.359 | 0.981 | 0.992 |
| Southern Hemisphere Sea Ice | 2.971 | 0.984 | 0.995 |
| Mean Northern Hemisphere | 3.497 | 0.985 | 0.989 |
| Mean Southern Hemisphere | 1.058 | 0.992 | 0.996 |
| Mean Northern and Southern Hemispheres | 5.959 | 0.973 | 0.971 |
| ***37h*** | **Intercept (K)** | **Slope** | **Correlation Coefficient (r)** |

| | | | |
|---|---|---|---|
| Greenland Ice Sheet | 6.139 | 0.967 | 0.991 |
| Antarctic Ice Sheet | 4.723 | 0.97 | 0.996 |
| Greenland and Antarctic Ice Sheets | 2.419 | 0.987 | 0.998 |
| Northern Hemisphere Sea Ice | 6.11 | 0.966 | 0.991 |
| Southern Hemisphere Sea Ice | 6.81 | 0.965 | 0.991 |
| Mean Northern Hemisphere | 1.607 | 0.994 | 0.998 |
| Mean Southern Hemisphere | 2.847 | 0.984 | 0.997 |
| Mean Northern and Southern Hemispheres | 1.501 | 0.993 | 0.998 |
| ***37v*** | **Intercept (K)** | **Slope** | **Correlation Coefficient (r)** |
| Greenland Ice Sheet | -3.28 | 1.015 | 0.993 |
| Antarctic Ice Sheet | -1.007 | 1.002 | 0.998 |
| Greenland and Antarctic Ice Sheets | -2.096 | 1.009 | 0.999 |
| Northern Hemisphere Sea Ice | 6.548 | 0.97 | 0.988 |
| Southern Hemisphere Sea Ice | 2.413 | 0.99 | 0.991 |
| Mean Northern Hemisphere | 2.659 | 0.989 | 0.991 |
| Mean Southern Hemisphere | -1.816 | 1.007 | 0.999 |

| | | | |
|---|---|---|---|
| Mean Northern and Southern Hemispheres | 4.099 | 0.982 | 0.989 |

It is apparent from Table 11 that the two data sets are highly correlated, with correlation coefficients greater than 0.98 for all cases. In general, the correlation coefficients are greater for the Southern than for the Northern Hemisphere. This is most likely a result of greater diurnal variability in the Northern Hemisphere during the months used in the analysis. For example, the scatter about the regression line is consistently greater for Greenland than Antarctica. Although the Greenland sample area was chosen to minimize melt effects, the melt signal in Greenland may reach altitudes over 2000m (Abdalati, personal communication). Also, atmospheric effects on brightness temperatures will typically be greater for the Greenland summer conditions than for the Antarctic winter. The fact that the lowest correlation occurs at the 22 GHz channel, the channel most sensitive to atmospheric conditions, likely reflects this. Similarly, slightly greater scatter about the regression line is seen for the Northern Hemisphere sea ice, reflecting the greater variability in sea ice and weather conditions during the time of year used in the analysis.

In Figure 8, the relative difference between F13 and F11 brightness temperatures, as a function of F11 brightness temperature, is shown using the combined ice sheet results and the individual Southern Hemisphere regions (designated as Antarctic Ice Sheet, Antarctic Sea Ice, and mean Southern Hemisphere [S]). Figure 9 illustrates that not only the magnitude, but also the direction of the adjustments to the F13 data differ depending on the choice of regression coefficients selected. In Figure 8, the same results are shown but for the Northern Hemisphere coefficients.

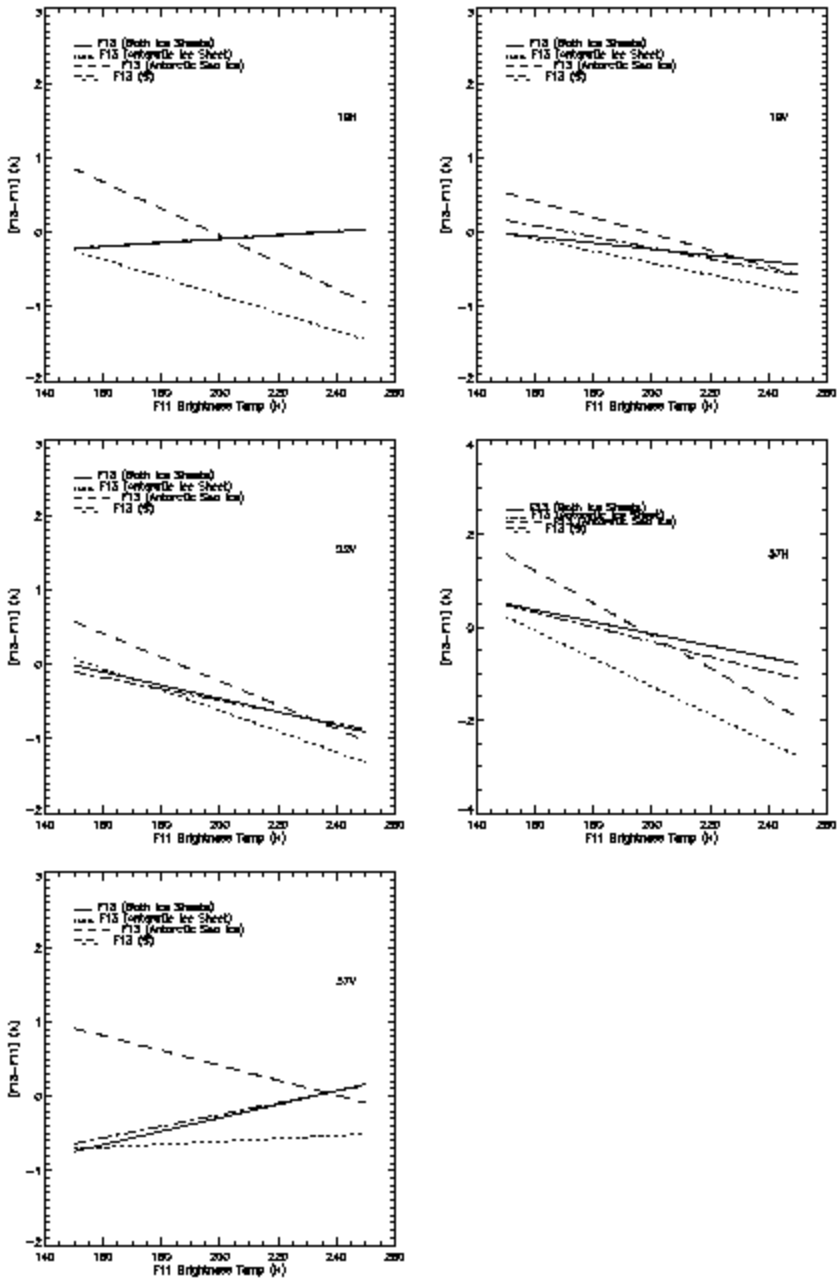


Figure 8. Relative difference between F13 and F11 brightness temperatures for the Southern Hemisphere using various regression coefficients.

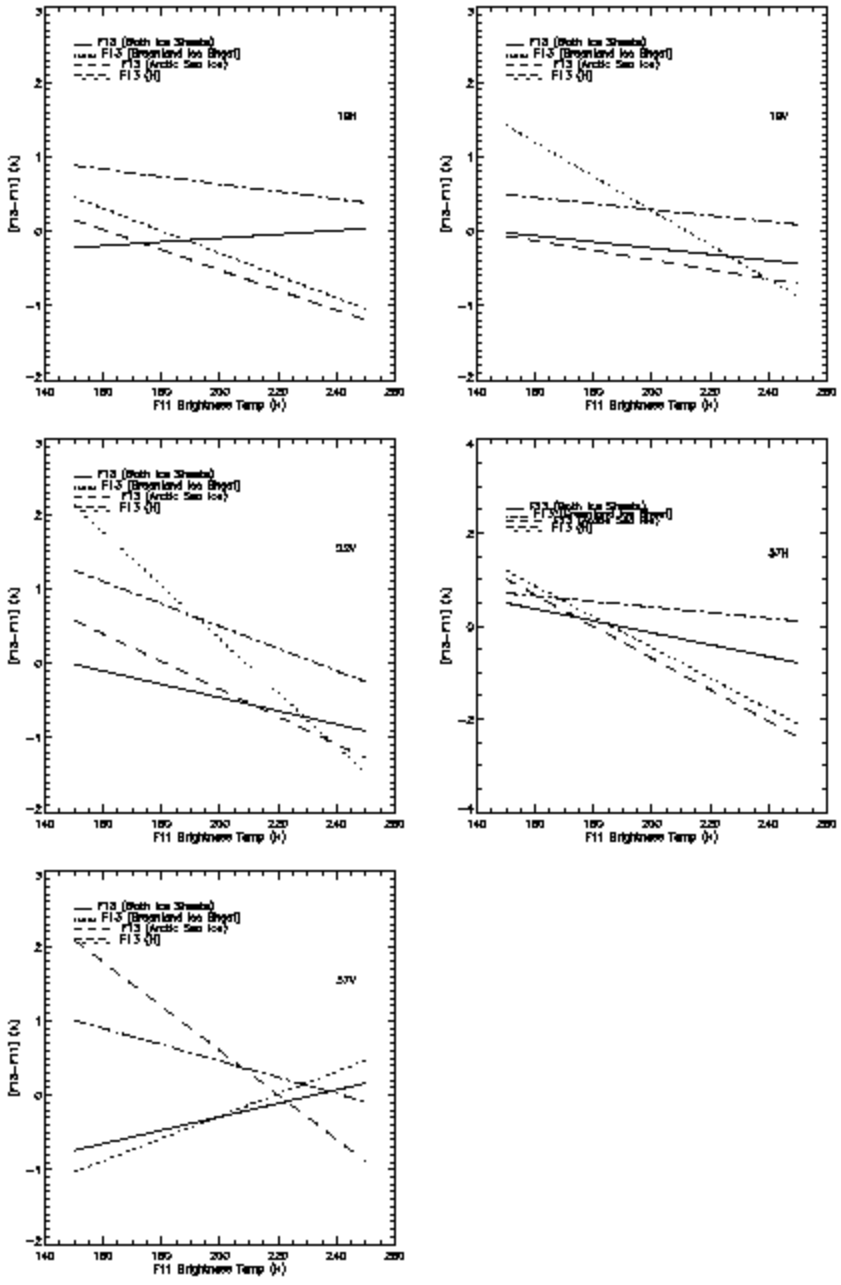

Figure 9. Relative difference between F13 and F11 brightness temperatures for the Northern Hemisphere using various regression coefficients.

# Effects of Brightness Temperature Adjustments on Ice Concentration Estimates

Even though the F11 and F13 brightness temperatures are highly correlated, with slopes near 1, the differences arising from the choice of sampling region could potentially have a significant effect on the resulting adjusted brightness temperatures and, in turn, ice concentrations calculated from these adjusted temperatures. The NASA Team sea-ice algorithm described

earlier is particularly sensitive to a decrease in the horizontally-polarized brightness temperature, which causes it to under-predict ice concentrations in certain cases (Smith 1996).

Using the combined ice-sheet-based coefficients, there is only a 0.2 K decrease in the relative difference between F11 and F13 19H brightness temperatures over a temperature range of 150 - 200 K. In contrast, using the Arctic sea ice coefficients, a 1.5 K increase in the relative difference at 19H is found. This results in different Northern Hemisphere summer sea ice fractions and suggests that ice-sheet-based coefficients estimated using the relatively low brightness temperatures typical of ice sheets are less valid for regions with greater brightness temperatures, such as Arctic sea ice during summer. Not surprisingly, we found that the Arctic sea-ice-based coefficients provided the best fit between the F11 and F13 ice fractions in the Northern Hemisphere and reduced the bias observed in the North and East Greenland seas. However, these coefficients caused much larger biases in the Southern Hemisphere. Using the combined ice sheet-based coefficients had a negligible improvement in consistency of ice fractions in the Southern Hemisphere, but slightly increased differences in the Northern Hemisphere.

Table 12 compares total ice fractions between the F11 and F13 satellites derived from brightness temperatures adjusted using regression coefficients from the (1) combined ice sheet, (2) combined sea ice, (3) mean Northern Hemisphere, (4) mean Southern Hemisphere and (5) combined mean Northern and Southern Hemisphere samples. Results are presented using the expanded land masks only. It is important to keep in mind that the statistics presented in Table 12 do not offer a complete picture of the overall differences. For example, use of the mean Northern Hemisphere-based coefficients causes the mean difference in the interior of the ice pack to be zero percent, but slightly increases the biases observed in the North and East Greenland seas so that the overall mean difference increased when compared with the unadjusted results given in Table 3. Similarly, using the combined ice sheet-based regression coefficients increases the differences in the interior of the ice pack, but reduces them over the open ocean and in the North Greenland Sea. With all sets of coefficients, statistically significant differences in ice fractions remain.

**Table 12. Comparison between F11 and F13 mean total ice fractions (F11 minus F13).**

| Area | Mean Difference (%) | Standard Deviation (%) | r.m.s. Error (%) | Correlation Coefficient (r) |
|---|---|---|---|---|
| ***Northern Hemisphere*** | | | | |
| Combined Ice Sheets | 0.06 | 0.83 | 0.81 | 0.999 |
| Combined Sea Ice | 0.19 | 0.83 | 0.82 | 0.999 |
| Mean Northern Hemisphere | 0.31 | 0.87 | 0.81 | 0.999 |
| Mean Southern Hemisphere | 0.08 | 1.17 | 0.95 | 0.999 |

| | | | | |
|---|---|---|---|---|
| Mean Northern and Southern | 0.83 | 1.40 | 0.96 | 0.999 |
| ***Central Arctic*** | | | | |
| Combined Ice Sheets | 0.10 | 1.21 | 1.18 | 0.999 |
| Combined Sea Ice | 0.23 | 1.20 | 1.19 | 0.999 |
| Mean Northern Hemisphere | 0.63 | 1.27 | 1.19 | 0.999 |
| Mean Southern Hemisphere | 0.49 | 1.99 | 1.48 | 0.999 |
| Mean Northern and Southern | 2.59 | 2.19 | 1.96 | 0.998 |
| ***Southern Hemisphere*** | | | | |
| Combined Ice Sheets | 0.05 | 0.74 | 0.71 | 0.999 |
| Combined Sea Ice | 0.09 | 0.74 | 0.72 | 0.999 |
| Mean Northern Hemisphere | 0.72 | 1.01 | 0.73 | 0.999 |
| Mean Southern Hemisphere | -1.47 | 1.81 | 1.32 | 0.999 |
| Mean Northern and Southern | 1.49 | 1.88 | 0.79 | 0.999 |

# Comparison of F8 and F11 Sea Ice Concentrations

The above results suggest that the use of any of the brightness temperature adjustments given in Table 11 does not offer an overall significant improvement in the consistency of ice fractions between the F11 and F13 platforms. The F11 ice products produced by NSIDC however, incorporate the F11 brightness temperature adjustments of Abdalati et al. (1995). More recent SSM/I data sets (e.g. new NASA Goddard Space Flight Center (GSFC) data set, EASE-Grid data set from NSIDC) apply the F11 antenna temperature adjustments from Wentz (1995). In light of the results noted above, it is important to reconsider the impact of these different adjustments on the F8 and F11 ice concentrations. Before discussing the impact of these adjustments on ice fraction estimates, there are some fundamental differences in the two types of adjustments that require mention.

As described earlier, Abdalati et al. (1995) used gridded, daily averaged brightness temperatures over cold ice sheets for their comparison. The period of overlap for F8 and F11 consists of only

16 days from 3 December to 18 December, 1991. The resulting regression equations are applied directly to gridded brightness temperatures. Wentz (1995) performs an intercalibration between F10 and F8 antenna temperatures, and between F11 and F10 antenna temperatures. For the F8 and F10 intercomparison, individual orbit crossovers are used to obtain near-simultaneous observations. In this way, errors due to random spatial-temporal variability and the diurnal cycle are minimized. In the F10-F11 intercalibration, the near-simultaneous crossovers occurred at 80 N and 80 S. Since data over the open ocean were preferred to those over sea ice, a region over the open ocean was selected that had a crossover time lag of 3.5 hours. Further adjustments are then needed to remove the diurnal cycle from the F10 and F11 antenna temperatures prior to any comparison.

Sea ice concentrations for both hemispheres were calculated here for the 16 days of overlap between the F8 and F11 sensors. The results of the mean (16-day) total ice concentrations for the Northern Hemisphere are presented in Figures 10 [a]-[c], using (1) no coefficients, (2) Abdalati et al. (1995) coefficients and (3) Wentz (1995) coefficients applied to the F11 brightness temperatures. While the application of the Wentz antenna temperature calibration coefficients to the brightness temperatures is not mathematically correct, the error is negligible (~0.001K).

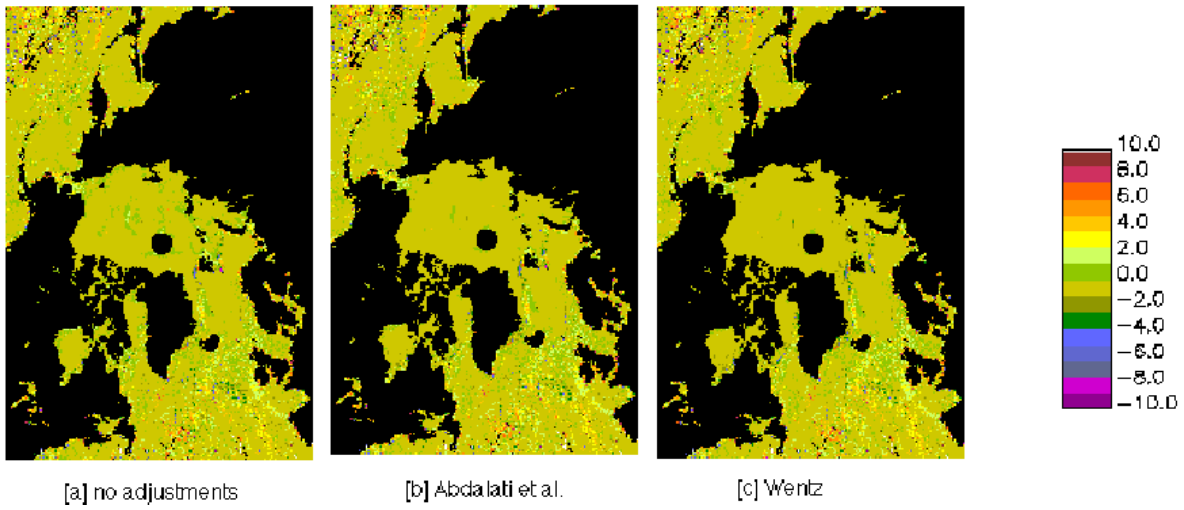


Figures 10 [a]-[c]. Spatial patterns of Northern Hemisphere total ice concentration differences.

Figures 11 [a]-[c] show the results for the Southern Hemisphere, with the statistics summarized for both hemispheres in Table 13. The values given in Table 13 were computed using the expanded land masks. As previously observed in Figure 1, the differences between the two satellites are greatest along the ice margin in the North and East Greenland seas, along the coasts (three to eight percent) and over the open ocean (10 percent). These biases remain after the coefficients of Abdalati et al. (1995) and Wentz (1995) have been applied to the F11 brightness temperatures and remain significant at a 99 percent confidence level.

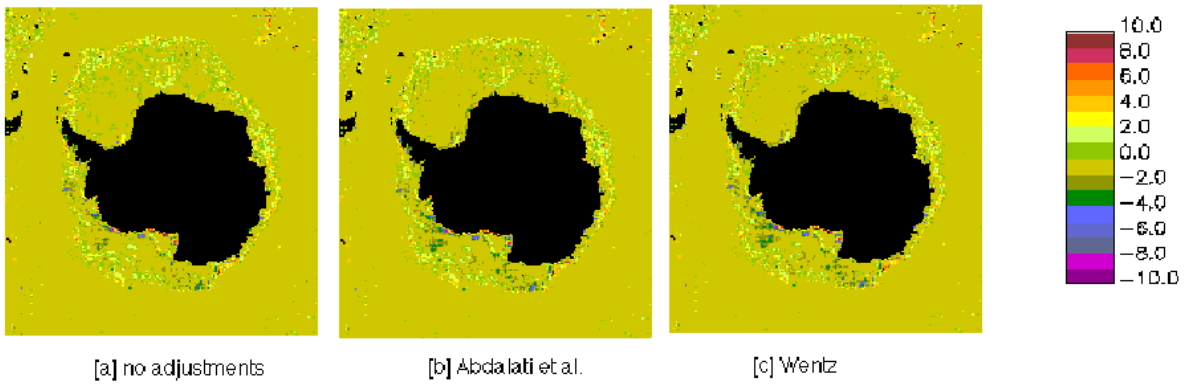


Figures 11 [a]-[c]. Spatial patterns of Southern Hemisphere total ice concentration differences.

In the Southern Hemisphere, larger differences are observed than were previously noted between F11 and F13. This is because the F8-F11 overlap occurs in polar summer in the Southern Hemisphere, resulting in larger orbital differences for the reasons cited earlier. Along the coasts, the differences are on the order of two to eight percent. In the interior of the ice pack, differences are smaller (one to three percent), but may be as large as four to six percent in the Amundsen and Ross seas. Differences at the ice edge range from one to six percent. The total ice concentration differences in the above mentioned locations are significant at a 99 percent confidence level.

In the Northern and Southern hemispheres, the adjustments serve to increase the magnitude of F11 total sea ice fractions, and increase overall mean differences in the Northern Hemisphere. Therefore, the smallest overall mean difference in the Northern Hemisphere total ice fraction between F8 and F11 is observed with no adjustments. However, slightly lower standard deviations and r.m.s. errors are found using the Abdalati et. al. (1995) or Wentz (1995) coefficients. The reverse is true in the Southern Hemisphere, where the adjustments slightly reduce the mean difference but increase the standard deviation and r.m.s. errors.

**Table 13. Comparison between F8 and F11 total ice fractions for the Northern Hemisphere, central Arctic and Southern Hemisphere after applying (1) no coefficients, (2) Abdalati et al. (1995) coefficients and (3) Wentz (1995) coefficients to the F11 data.**

| Description | Mean Difference (%) | Standard Deviation | r.m.s. error (%) | Correlation Coefficient (r) |
|---|---|---|---|---|
| **Northern Hemisphere** | | | | |
| None | -.02 | 1.82 | 1.82 | 0.998 |
| Abdalati et al. (1995) | -0.23 | 1.81 | 1.8 | 0.998 |
| Wentz (1995) | -0.25 | 1.81 | 1.79 | 0.999 |
| **Central Arctic** | | | | |

| | | | | |
|---|---|---|---|---|
| None | 0.13 | 1.43 | 1.42 | 0.999 |
| Abdalati et al. (1995) | -0,24 | 1.43 | 1.43 | 0.999 |
| Wentz (1995) | -0.05 | 0.69 | 0.58 | 0.999 |
| **Southern Hemisphere** | | | | |
| None | 0.12 | 1.25 | 1.25 | 0.999 |
| Abdalati et al. (1995) | 0.04 | 1.29 | 1.27 | 0.999 |
| Wentz (1995) | 0.02 | 1.29 | 1.27 | 0.999 |

In the central Arctic, the Wentz (1995) adjustments result in the overall lowest mean difference, standard deviation and r.m.s. error. From Figures 10 [a]-[c] we notice that the differences in the interior of the ice pack slightly decrease using the Abdalati et al. (1995) and Wentz (1995) adjustments, while differences in the North and East Greenland seas increase. In general, in the Northern Hemisphere the F11 total ice-covered area is slightly greater than is true for F8, and in the Southern Hemisphere, total ice-covered area is slightly less for F11 when compared to F8 data.

Figures 12 [a]-[c] and Table 14 summarize the 16-day mean differences in multiyear ice concentrations for the Northern Hemisphere. Again, similar discrepancies between the two satellites are observed in the North and East Greenland seas (two to six percent), but there are also locations within the interior of the icepack (e.g., directly north of the pole) with differences of the same magnitude. The smallest MYI mean differences, standard deviations and r.m.s. errors between F8 and F11 are found using no adjustments. This is true for the entire Northern Hemisphere grid and the central Arctic region. The mean differences, standard deviations and r.m.s. errors all increase when limiting the analysis to the central Arctic. The same result was noted previously in the F11/F13 MYI fraction comparison, and is a result of MYI biases being virtually nonexistent over the open ocean.

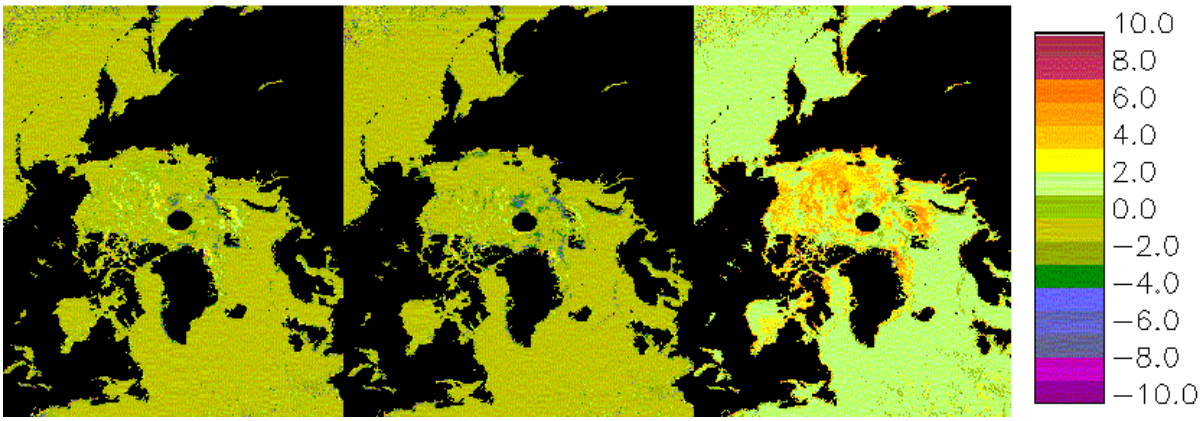


Figures 12 [a]-[c]. Spatial patterns of Northern Hemisphere multiyear ice concentration differences.

**Table 14. Comparison between F8 and F11 multiyear ice fractions for the Northern Hemisphere and central Arctic after applying (1) no coefficients, (2) Abdalati et al. (1995) coefficients and (3) Wentz (1995) coefficients to the F11 data.**

| Description | Mean Difference (%) | Standard Deviation | r.m.s. error (%) | Correlation Coefficient (r) |
|---|---|---|---|---|
| **Northern Hemisphere** | | | | |
| None | -0.03 | 0.77 | 0.77 | 0.999 |
| Abdalati et al. (1995) | -0.16 | 0.79 | 0.79 | 0.999 |
| Wentz (1995) | 0.22 | 0.91 | 0.83 | 0.999 |
| **Central Arctic** | | | | |
| None | 0.03 | 1.69 | 1.69 | 0.998 |
| Abdalati et al. (1995) | -0.55 | 1.69 | 1.69 | 0.998 |
| Wentz (1995) | 0.92 | 1.81 | 1.79 | 0.998 |

In Table 15 we compare the total sea-ice covered area and extent. No statistically significant mean differences are found in the total ice covered area for the Northern Hemisphere between F8 and F11 (unadjusted). Since the adjusted F11 data cause the total ice fraction, and hence total ice-covered area amount to increase, the mean difference in ice covered area in the Northern Hemisphere increases from -0.06 percent to -0.43 percent with the Abdalati et al. (1995) and to -0.87 percent with the Wentz (1995) coefficients. These differences are statistically significant for a 99 percent confidence level and are a result of the mean differences in total ice fraction increasing with both sets of adjustments (see Table 13). The same result is observed in the central Arctic. In the Southern Hemisphere, the much larger discrepancies in total sea ice-covered area are statistically significant, with the unadjusted F11 performing better relative to F8.

**Table 15. Comparison of mean differences in total sea ice extent and total sea ice covered area**
**between the F8 and F11 satellites (F8 minus F11) after applying (1) no coefficients, (2) Abdalati et al. (1995) coefficients and (3) Wentz (1995) coefficients to the F11 data.**

| Description | Mean Difference ($km^2$) | Standard Deviation ($km^2$) | Maximum Difference ($km^2$) | Minimum Difference ($km^2$) |
|---|---|---|---|---|
| **Ice Area** | | | | |

| | | | | |
|---|---|---|---|---|
| **Northern Hemisphere** | | | | |
| No adjustments | -6.282 (-0.06%) | 32,852 | -54,101 | 56,800 |
| Abdalati et al. (1995) | -46,593 (-0.43%) | 32,999 | -93,001 | 22,500 |
| Wentz (1995) | -92,710 (-0.87%) | 34,299 | -140,201 | -17,459 |
| **Central Arctic** | | | | |
| No adjustments | 10,178 (-0.13%) | 17,079 | -17,490 | 41,440 |
| Abdalati et al. (1995) | -29,395 (-0.38%) | 16,084 | -52,820 | 1,800 |
| Wentz (1995) | -61,110 (-0.79%) | 17,165 | -81,219 | -15,950 |
| **Southern Hemisphere** | | | | |
| No adjustments | -36.298 (-0.49%) | 44,763 | -90,090 | 60,010 |
| Abdalati et al. (1995) | -79,855 (-1.09%) | 45,820 | -134,620 | 25,850 |
| Wentz (1995) | -89,405 (-1.23%) | 48,916 | -145,910 | 24,370 |
| **Ice Extent** | | | | |
| **Northern Hemisphere** | | | | |
| No adjustments | -124,922 (-0.97%) | 105,305 | -296,875 | 58,750 |
| Abdalati et al. (1995) | -42.929 (-0.33%) | 82,140 | -172,500 | 109,375 |
| Wentz (1995) | -35.078 (-0.27%) | 71,472 | -155,625 | 86,250 |
| **Central Arctic** | | | | |
| No adjustments | -6,015 (-0.07%) | 28,486 | -89,375 | 29,375 |
| Abdalati et al. (1995) | 1,875 (0.02%) | 26,083 | -68,750 | 42,500 |
| Wentz (1995) | 78 (0.009%) | 23,698 | -53,125 | 45,625 |
| **Southern Hemisphere** | | | | |
| No adjustments | -41,015 (-0.38%) | 46,588 | -116,875 | 33,125 |
| Abdalati et al. (1995) | -9,336 (-0.08%) | 47,342 | -71,875 | 111,250 |
| Wentz (1995) | -976 (-0.009%) | 52,594 | -84,375 | 128,125 |

In terms of total ice extent however, the coefficients do offer a substantial improvement. The difference between unadjusted F11 and F8 ice extent in both hemispheres is statistically significant, whereas the adjusted F11 values are not. For both hemispheres, and for the central Arctic, the Wentz (1995) adjustments provide the best fit in term of sea ice extent.

# Summary and Conclusions

There remain significant differences in ice fractions, ice extent and ice covered area between the DMSP F8, F11 and F13 satellites that are not removed through simple linear adjustments to the brightness temperatures. Pronounced biases persist in the East and North Greenland seas, along the ice margins and along the coasts. The biases along the coasts can be reduced using an expanded land mask. An ocean mask may also be applied to mask out the large differences in ice fraction over the ocean where false ice concentrations result from weather effects. Another possibility would be to change the weather filter criteria from platform to platform. The current criteria of the weather filter is that if the gradient ratio between 37 and 19 GHz is greater than 0.05, and/or the gradient ratio between 22 and 19 GHz is greater than 0.045, the sea ice concentration is set to zero. A count of the number of pixels in the images that meet this requirement for F11 and F13 indicates that more pixels are classified as open water by the weather filter for the F11 satellite. A slight tuning of the weather filter thresholds as applied to F13 would reduce this difference.

Even though the brightness temperatures from the different SSM/I sensors are highly correlated, an extended time series involving the two instruments is affected by the differences between the instruments. The magnitude of these differences depends on the parameter of interest (total ice, multiyear ice, total ice extent, etc.), whether specific regions are being studied, and on the kind of adjustments, if any, that are applied to the brightness temperatures. Our comparisons do not suggest a single, globally applicable, regression-based adjustment to uniformly improve the match between brightness temperatures from the different SSM/I instruments. This may indicate some non-linearity in the intercalibration among the instruments, although we were unable to detect any such non-linearity. Instead, the differences in regression fits using the different choices of data samples (e.g., ice sheets, Northern vs. Southern Hemisphere, etc.) may be due to random variability in the data. The NASA Team algorithm is sensitive enough to these slight differences to yield significant differences in ice concentrations resulting from the choice of regression coefficients. For the data studied, these differences are not large enough to have a substantial impact on the monitoring of global sea ice trends using F8, F11, and F13. However, data users focusing on a specific region and time should be alert to the points in the time series when the sensors change, and should weigh the differences discussed here versus apparent physical changes in ice conditions.

While the identification of a globally-applicable set of adjustments is desirable from a theoretical and practical point of view, it is clear that simple steps such as minimizing land contamination and open-ocean differences go far toward reducing the observed differences in derived ice concentrations. Brightness temperature adjustments specific for certain regions and/or conditions will likely improve agreement for particular situations, but it must be recognized that such adjustments are seen to cause greater differences elsewhere. We also emphasize that any adjustments based on the overlapping time periods among the data may be less accurate for other times of year, and could conceivably introduce unknown biases under the different conditions present in other seasons.

All of these caveats should be considered before any adjustments are used. The physicians' creed of "First, do no harm" should be borne in mind in this case. Perhaps the safest approach is to tailor the adjustment procedure to the parameter of interest (Zabel and Jezek 1994) with clear indication that the adjustment may not be suited to other applications. In the case of sea ice concentrations, this could include applying land and ocean masks in combination with adjustments to algorithm tie points, or the use of regression adjustments between ice concentrations derived from the different SSM/I sensors. This latter approach has been used by NASA GSFC to produce a combined SMMR - SSM/I F8 through F11 time series of ice concentrations now available from NSIDC. It might also be necessary to adjust the algorithm tie points for each sensor, as they are based on observed brightness temperatures and therefore depend on the microwave sensor. However, until further comparisons are done between F11 and F13, NSIDC has chosen to apply no adjustments to the brightness temperatures used to generate F13 ice concentrations, or to the F13 ice concentrations themselves.

Finally, we note that work remains to be done to examine the effects of changing sensors on SSM/I 85 GHz data and on other passive microwave algorithms for sea ice and snow. However, the brightness temperature comparisons given here provide some indication of at least the sign of changes due to sensor differences. For example, we noted that the F11 - F13 differences were greatest between frequencies (e.g., 19 GHz vs. 37 GHz) than between polarizations. For the NASA Team algorithm, this translated into larger errors for discrimination of ice type than for ice concentration. Snowcover algorithms that typically rely on the 19 vs. 37 gradient will likely be similarly affected.

# Acknowledgments

This work was supported by the NASA EOS program.

# References

Abdalati W., K. Steffen, C. Otto and K. Jezek. 1995. Comparison of brightness temperatures from SSM/I instruments on the DMSP F8 and F11 satellites for Antarctica and the Greenland ice sheet. *Int. J. Remote Sens*. 16:1223-1229.

Cavalieri, D.J., K. St. Germain and C.T. Swift. 1995. Reduction of weather effects in the calculation of sea ice concentration with the DMSP SSM/I. *J. Glaciology*. 41:455-464.

Cavalieri, D. J., J. Crawford, M. Drinkwater, W. J. Emery, D. T. Eppler, L. D. Farmer, M. Goodberlet, R. Jentz, A. Milman, C. Morris, R. Onstott, A. Schweiger, R. Shuchman, K. Steffen, C. T. Swift, C. Wackerman, and R. L. Weaver. 1992. NASA sea ice validation program for the DMSP SSM/I: final report. **NASA Technical Memorandum 104559**. National Aeronautics and Space Administration, Washington, D.C. 126 pages.

Gloersen, P., and D.J. Cavalieri. 1986. Reduction of weather effects in the calculation of sea ice concentration from microwave radiances. *J. Geophys. Res*. 91:3913-3919.

Jezek, K.C., C. Merry, D. Cavalieri, S., Grace, J. Bedner, D. Wilson and D. Lampkin. 1991. Comparison between SMMR and SSM/I passive microwave data collected over the Antarctic ice

sheet. *Byrd Polar Research Center Technical Report No. 91-03*. The Ohio State University, Columbus.

Johannessen, O.M., M. Miles, and E. Björgo. 1995. The Arctic's shrinking sea ice. *Nature*. 376:126-127.

Maslanik, J.A., M.C. Serreze, and R.G. Barry. 1996. Recent decreases in Arctic summer ice cover and linkages to atmospheric circulation anomalies. *Geophys. Res. Lett.* 23:1677-1680.

NSIDC. 1996. *DMSP SSM/I Brightness Temperatures and Sea Ice Concentration Grids for the Polar Regions: User's Guide*. NSIDC Distributed Active Archive Center.

Parkinson, C.L. 1992. Spatial patterns of increases and decreases in the length of the sea ice seasons in the north polar region, 1979-1986. *J. Geophys. Res.* 97:14377-14388.

Parkinson, C.L. and D.J. Cavalieri. 1989. Arctic sea ice 1973-1987: seasonal, regional, and interannual variability. *J. Geophys. Res.* 94:14,499-14,523.

Smith, D.M. 1996. Extraction of winter total sea-ice concentration in the Greenland and Barents Seas from SSM/I data. *Int. J. Remote Sens.* 17:2625-2646.

Wentz, F. 1995. Deriving Earth science products from SSM/I. *Progress Report for Contract NASA-4714, August 1993 through January 1995*, 2-4.

Zabel, I.H., and K.C. Jezek. 1994. Consistency in long-term observations of oceans and ice from space. *J. Geophys. Res.* 99:10109-10121.